https://doi.org/10.1016/j.ijmecsci.2019.06.032

An analytical force model for ultra-precision diamond sculpturing of micro-grooves with textured surfaces

Zhanwen Sun[a,b], Suet To[b,*], Sujuan Wang[a]

[a] *State Key Laboratory of Precision Electronic Manufacturing Technology and Equipment, Guangdong University of Technology, Guangzhou, China*

[b] *State Key Laboratory in Ultra-precision Machining Technology, Department of Industrial and Systems Engineering, The Hong Kong Polytechnic University, Kowloon, Hong Kong*

** Corresponding author at: The Hong Kong Polytechnic University, Department of Industrial and Systems Engineering, State Key Laboratory in Ultra-precision Machining Technology, Kowloon, Hong Kong. Email：* sandy.to@polyu.edu.hk*; Tel: +852 2766 6587; Fax: +852 2764 7657*

Abstract

The investigation on the cutting force for ultra-precision diamond sculpturing (UPDS) is important to understand its material removal mechanism and tool-workpiece reaction behaviors during cutting. However, few studies have focused on the cutting force model for UPDS of micro-grooves with textured surfaces. The prediction of the cutting force for UPDS is complicated due to its unique kinematics featuring oscillated servo motions, which inevitably leads to the dynamic material removal process featuring time varying plastic deformation directions. In the present study, an analytical cutting force model for UPDS of textured micro-grooves is proposed with the full consideration of the oscillations induced dynamic cutting conditions, round-edged effect as well as the shearing and ploughing mechanisms. Specifically, the nominal shearing force is derived by a dynamic slip-line model involving the time varying shear angle, stress, strain and strain rate in the deformation zone. A two-state model is adopted to describe sticking and sliding states of the chip on the tool rake face, based on which the frictional shearing force is calculated. When the depth of cut is lower than the critical chip thickness, the material is removed by the ploughing force that is of proportional relation to the tool-workpiece interference volume according to the indentation theory. Finally, the whole cutting force is obtained by discretization method, and the model is experimentally validated through sculpturing two types of textured micro-grooves with harmonic structures.

Keywords: Cutting force model; Diamond sculpturing process; Micro-structures; material removal mechanism

Nomenclatur		t_i	Time of the *i*-th CLP Width
e o_w-$x_w y_w z_w$	Coordinate system fixed on	$w_{i,j}$	of the *j*-th discretized

	workpiece		element
o_t-$x_t y_t z_t$	Coordinate system fixed on tool	σ_s	Equivalent shear stress Equivalent
$(y_{CLP}^{i}, z_{CLP}^{i})$	Coordinate of the *i*-th CLP	ε_s	shear strain Equivalent shear strain
$F(\cdot)$	Function of cutting trajectory	$\dot{\varepsilon}_s$	rate
R_t	Tool nose radius	τ_s	Shear stress
r_e	Tool edge radius	τ_f	Frictional stress
$\gamma_{i,j}$	Equivalent rake angle	γ_s	Shear strain
$\gamma_e^{i,j}$	Edge shape induced rake angle	$\dot{\gamma}_s$	Shear strain rate
γ_0	Tool rake angle	$\gamma_s^{i,j}$	Shear strain
$\kappa_{i,j}$	Equivalent clearance angle	$\dot{\gamma}_s^{i,j}$	Shear strain rate
κ_0	Tool clearance angle	$F_n^{i,j}$ $F_f^{i,j}$	Normal force and friction force
$\phi_{i,j}$	Equivalent shear angle at *i*-th CLP and *j*-th discretized element	$F_{c,s}^{i,j}$ $F_{t,s}^{i,j}$	Cutting and thrust force at *i*-th CLP and *j*-th discretized element Plough
$\phi_d^{i,j}$	Effective shear angle induced by changed cutting velocity Effective	$F_{c,p}^{i,j}$ $F_{t,p}^{i,j}$	forces in cutting and thrust directions
ϕ_p	shear angle induced by waviness of previous-cut surface Equivalent	F_t^i F_c^i	Thrust and cutting force at the *i*-th CLP
ζ_1 ζ_2	ratios of the DoC to chip thickness	*A B C m n*	Johnson-Cook model related parameters
$v_s^{i,j}$	Velocity along the shear plane	ρ	Density of workpiece material (g/cm^3)
$l_{AB}^{i,j}$	Length of shear plane	*S*	Material specific heat (J/kg·°C)
C_0	Parameter determined by material properties	s_1 s_2	Distance along the shear band and vertical to shear band
T, T_m T_0	working temperature, melting temperature and room temperature (°C)	ξ	Coefficient determining equivalent height of tool-chip contact area
u_p	Ploughing friction coefficient	β	Heat diffusion coefficient
$\Psi_{i,j}$	Inclination angle between the	μ_e	Friction coefficient on tool rake

	equivalent rake face and the *z*-axis		face
σ_{A} σ_{B}	Hydrostatic stress on the two ends of the shear band	v_r	Resultant cutting velocity
μ_p	Ploughing friction coefficient	v_y^i v $\frac{i}{z}$	Cutting velocity in *y*- and *z-axis*
N	Number of the discretized elements	Δy	Discretized interval of trajectory
$\theta_{i,j}$	Relative angle of the *j*-th element	$d_{i,j}$	Practical depth of cut
$\varsigma_{i,j}$	Angle determined by practical depth of cut	k_{int}	Proportion ratio of the ploughing force
l_c	Contact length of the chip on tool rake face	$\vartheta_{i,j}$	Inclination angle between the thrust direction and the *z*-axis
a	Parameter determining the stress distribution	u	Distance to the tool edge lowest point
l_s	Sticking length of the chip on tool rake face	$V_{i,j}$	Tool-workpiece interference volume

1. Introduction

Micro-grooves with textured surfaces have attracted increasing attention in a variety of industrial applications, such as biological medicine, MEMS and plasma fluidic control [1, 2]. Ultra-precision diamond sculpturing (UPDS) has been demonstrated to be a very promising technique to achieve flexible fabrication of textured micro-grooves with high form accuracy [3-5]. In UPDS, the diamond tool precisely follows a space trajectory controlled by the associated servo motions in both feed and depth-of-cut (DoC) directions. Textured surfaces are accordingly generated by directly imprinting the tool edge shape on the workpiece surface. Through properly planning the tool trajectory, micro-grooves with desired textured surfaces can be generated by UPDS with high flexibility and form accuracy.

Cutting force directly reflects the material removal mechanism and tool-workpiece reaction behaviors in the deformation zone, so the investigation on the cutting force for UPDS is the premise of predicting tool wear, finished surface quality and tool tip vibration. Modelling of the cutting force for UPDS also help to achieve some innovative applications of this technology. For example, cutting force signals are currently used as the feedback of the cutting loop in order to improve the machining accuracy of micro-structures, which is named as force-controlled servo machining systems by

researchers [6, 7]. To achieve the force-controlled servo machining, accurate prediction of the generated cutting forces for UPDS is essentially required through modelling methods. However, the current force models applied on force-controlled systems are mostly developed on the basis of a simple assumption that the cutting force is proportional to the tool-workpiece engagement area, accordingly, having limited accuracy especially for complicated micro-structures [8]. Besides, few studies have focused on modelling the cutting force of UPDS with the consideration of material properties and dynamic cutting conditions.

Even though the cutting force generated in UPDS of textured micro-grooves was little investigated, extensive models have been proposed to predict the cutting force for milling and turning process [9-11]. For example, an analytical cutting force model was developed by Weng et al. [9] to predict the turning forces of round insert with the consideration of the edge effect. Oneunified model that is capable of predicating forces in turning and milling process was proposed by Kaymakci et al. [10] through transforming the insert geometry-dependent normal forces into a common reference frame followed by the operation specific machine coordinates. Currently, with the consideration of the kinematics and tool helix angle effect, a physics-based cutting force model was proposed by Verma et al. [11] to predict the static machining force in vibration-assisted milling process. Depending on the modelling theories, these models can be divided into three types, namely empirical, mechanistic and analytical models [12]. Empirical models estimate cutting forces through multiplying the material removal volume with a cutting force coefficient that is normally determined on the basis of experimental results [13, 14]. Without fully understanding the material removal mechanisms, both empirical and mechanistic models require numerous experiments to obtain reliable force coefficient, which is low-efficient and has limited universal application in other cases [12, 15]. In comparison, analytical models that are derived from material properties, mechanics and thermal-physics are more practical and scientific, as these models in-depth reveal the material removal mechanisms and tool-workpiece reaction behaviors in the deformation zone.

The pioneering work of the analytical force model proposed by Merchant [16] predicted the cutting force for orthogonal cutting through confining material plastic deformation along a single shearing plane. Even though this model is over-simplified without considering some important parameters, such as the mechanical properties of workpiece material, cutting speed and temperatures, it has a profound influence on the following researches in cutting force estimation. Currently, analytical

models have developed with an overall combination of many theories and factors, such as refined slip-line models, constitutive relationship of the workpiece material, lubrication state, temperature and material thermo-physical properties [17, 18]. These models proved an efficient approach to predict the cutting forces with high accuracy for various cutting processes, such as milling [19], turning [20, 21] and orthogonal cutting [22]. However, current analytical models cannot be directly used to estimate the cutting force for UPDS of textured surface, due to the none consideration of the unique cutting kinematics of UPDS featuring oscillated cutting process which inevitably results in dynamic material removal behavior. In UPDS, the oscillations induced time varying cutting directions lead to the time varying equivalent rake angle, shear angle, strain and stress in the deformation zone, and these dynamic factors need to be involved in the modelling of cutting force to ensure the prediction accuracy. Therefore, a comprehensive cutting force model considering the oscillations induced time varying cutting directions and the resulting dynamic material removal behavior is required for UPDS, in order to provide an in-depth understanding of the dynamic material removal mechanism of UPDS as well as to accurately predict the cutting force.

In the last few decades, slip-line theory has greatly developed through ever-refining the deformation zone to precisely simulate the metal cutting process. For example, developed from the Oxley's model, Li et al. [19] proposed an orthogonal cutting theory in which the shear zone is an unequally devised to simulate the non-uniform distribution of the temperature, strain and stress in the primary deformation zone. Moreover, through employing a curved shear band with multiple control angles, a slip-line model was proposed by Fang et al. [23] to determine important parameters of chip formation. To model the ploughing force induced by the edge shape, the plastic deformation zone was further divided into multiple sub-regions by Waldorf et al. [24]. Even though these models can describe the plastic deformation with high quality, the refined process can make the cutting force estimation very complicated and low-efficient, and is difficult to fulfil the real-time requirement of force-controlled system.

The motivation of this study is to develop a comprehensive analytical model for predicting the cutting force for UPDS of textured micro-grooves with the full consideration of the oscillated motions of the tool and its induced dynamic material removal process. Developed from the Oxley's model with single shear band, a dynamic slip-line model involving the time varying equivalent rake angle, shear angle, strain and stress is proposed to derive the dynamic normal shear stress in the deformation zone.

Noteworthy, although more refined slip-line models have been proposed to precisely simulate the metal cutting, Oxley'smodel is the most widely used one, and Oxley'smodel has been demonstrated to be applicable to transient cutting processes with high accuracy, such as milling [25, 26]. For example, Young et al. [25] and Pang et al. [26] have accurately predict the transient cutting forces in milling based on the model developed from Oxley'smodel. Through investigating the frictional states between the chip and the tool rake face, the frictional shear stress is derived by a two-state model. When the DoC is lower than the critical chip thickness, the material is removed by the ploughing force that is derived according to the indentation theory. By employing discretization method, the distribution of cutting force on tool edge is obtained, and the whole cutting force of UPDS can be calculated through summarizing all the force components of the discretized elements along tool edge. The proposed analytical model is experimentally validated by sculpturing two types of harmonic micro-grooves.

2. Kinematics for UPDS of textured micro-grooves

The schematic illustration of the kinematics in diamond sculpturing of textured micro-grooves is shown in Fig. 1. In UPDS, the diamond tool feeds along *y*-axis and simultaneously oscillates along *z*-axis to generate the textured surfaces, so the kinematics of UPDS is a kind of two-dimensional movement with one independent degree of freedom. Through deliberately planning the tool trajectory, micro-grooves with various textured surfaces can be flexibly fabricated with the assistance of the oscillated servo motions in both feed and depth-of-cut (DoC) directions. To mathematically describe the kinematics of UPDS, a coordinate system o_w-$x_w y_w z_w$ is built on the workpiece, and y_w-axis is assigned to feed direction. As the profile of the tool edge is imprinted on the micro-grooves during sculpturing, the surface of textured micro-grooves can be expressed by a general formula as:

$$z_s = F(y_w) + \left(R_t - \sqrt{{R_t}^2 - {x_w}^2}\right) \cos\gamma_0 \tag{1}$$

where $F(\cdot)$ is the function that describe the cutting trajectory of the diamond tool, R_t is the tool nose radius and γ_0 is tool rake angle. The function $F(y_w)$ describing the oscillated cutting trajectory of the diamond tool is the function of the coordinate y_w.

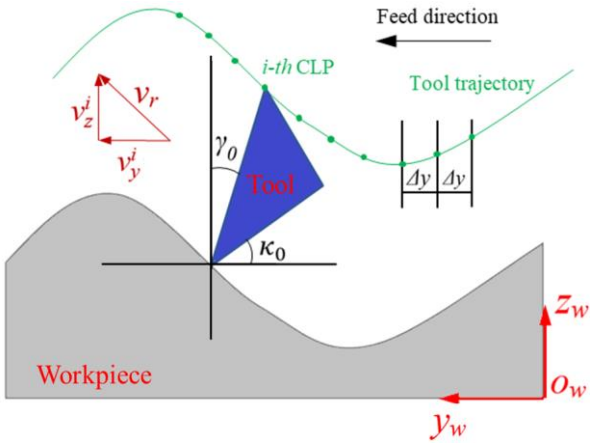

Fig. 1. Schematic of the kinematics for UPDS of textured micro-grooves.

For a round-edged diamond tool, the cutter location point (CLP) is normally set at the center of the tool nose on tool rake face, as shown in Fig. 1. The trajectory for UPDS is discretized with an equal interval Δy, so the coordinate of the *i*-th CLP can be expressed by:

$$\begin{cases} y_{CLP}^i = y_i - R_t \cdot sin\gamma_0 \\ z_{CLP}^i = F(y_i) + R_t \cdot cos\gamma_0 \end{cases} \tag{2}$$

with

$$y_i = \Delta y(i-1) \tag{3}$$

For any desired textured micro-grooves described by Eq. 1, the corresponding trajectory of CLPs can be determined by Eq. 2. In sculpturing process, the cutting speed along the tool trajectory is preset and remains unchanged. Due to the fluctuation of the textured surfaces, the cutting direction of the tool inevitably changes with respect to the local slope of the desired surface in UPDS, as shown in Fig. 1. To make the resultant cutting velocity v_r to be always same with the preset value, fast oscillations accordingly generate on the velocity components along *y*- and *z-axis*, which can be expressed by:

$$\begin{cases} v_y^i = cos\left(arctan\left(\dfrac{dF(y_i)}{dy}\right)\right) v_r \\ v_z^i = sin\left(arctan\left(\dfrac{dF(y_i)}{dy}\right)\right) v_r \end{cases} \tag{4}$$

Thus, it is learned that the kinematics for UPDS of micro-grooves with textured surfaces is more complicated with that ordinary orthogonal cutting. The time varying cutting directions of the resultant cutting velocity in UPDS inevitably leads to the dynamic material removal mechanisms, which should be considered in the modelling of cutting forces.

Through the integration method, the corresponding time of the *i*-th CLP can be determined as:

$$t_i = \frac{\int_0^{y_{CLP}^i} \sqrt{1 + \left(\frac{dF}{dy}\right)^2}\, dy}{v_r} \tag{5}$$

3. Analytical force model for UPDS

In the modelling of the cutting force for UPDS, discretization method is adopted on the tool edge, and each discretized element is regarded as a dynamic orthogonal cutting process following the oscillated servo motions of UPDS. The normal shearing force generated by the plastic deformation in the cutting zone is determined by a dynamic slip-line model that incorporates the oscillations induced dynamic cutting conditions of UPDS. The segmented frictional states along tool-chip interface is described by a two-state model considering both the sticking and sliding states, based on which the frictional shearing force is derived. For the discretized elements having a comparative DoC with tool edge radius, indentation theory is adopted to calculate the ploughing force in this case. Finally, through summarizing the force components of each discretized elements along tool edge, the total cutting force is acquired at each CLP.

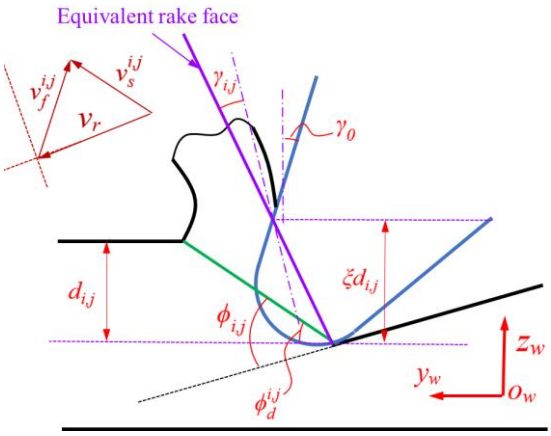

Fig. 2. Schematic of the dynamic slip-line model considering the cutting direction.

3.1 Shearing force model

To accurately predicting the cutting forces in UPDS of textured surfaces, the dynamic material removal mechanism induced by the oscillated servo motions is integrated into the modelling of shearing forces. Developed from the Oxley's model for machining metal materials, a dynamic slip-line model with straight shear plane is proposed to determine the position dependent plastic flow stress for UPDS considering the time varying cutting directions. The proposed shearing force model is used to calculate the cutting force for the discretized elements in the case that the practical DoC is larger than

the critical chip thickness.

3.1.1 Calculation of position dependent plastic flow stress

A schematic illustration of the dynamic slip-line model considering the time varying cutting directions is shown in Fig. 2. It is worth to note that the time varying cutting directions in UPDS lead to the dynamic material plastic deformation directions, so the geometrical relations shown in Fig. 2 for the proposed dynamic slip-line model is different from the conventional ones. Different from conventional orthogonal cutting with constant DoC, the equivalent rake angle of UPDS is not only determined by the tool rake angle, but also changes depending on the instantaneous cutting direction. Moreover, when the DoC is comparable to the tool edge radius, negative rake angle will be generate induced by the round edge shape [27]. With the overall consideration of the tool rake angle as well as the time varying cutting directions and practical DoCs, the equivalent rake angle in UPDS at the *i*-th CLP and the *j*-th discretized element can be expressed by:

$$\gamma_{i,j} = \gamma_0 + \gamma_e^{i,j} - arctan\,(\frac{dF(y_i)}{dy}) \tag{6}$$

where γ_0 is the tool rake angle and $\gamma_e^{i,j}$ is the effective rake angle induced by the tool edge shape, which can be expressed by [28]:

$$\gamma_e^{i,j} = arctan\,(\frac{u_{i,j}}{\xi d_{i,j}}) \tag{7}$$

where $d_{i,j}$ is the practical DoC of the discretized element and ξ is the parameter that determines the equivalent height of the tool-chip contact area, which should be larger than 1. The equivalent rake angle is acquired by drawing a straight line between the lowest point of the tool edge and a point on the tool rake face marking the equivalent chip contact height, as shown in Fig. 2. According to the geometric relation, $u_{i,j}$ can be expressed by:

$$u_{i,j} = \begin{cases} r_e\,cos\,[arcsin\,(\dfrac{r_e - \xi d_{i,j}}{r_e})\,] & \xi d_{i,j} \le r_e(1 + sin\,\gamma_0) \\ r_e\,cos\,\gamma_0 - \dfrac{\xi d_{i,j} - r_e}{cot\,\gamma_0} & \xi d_{i,j} > r_e(1 + sin\,\gamma_0) \end{cases} \tag{8}$$

where r_e is tool edge radius.

Shear angle is also an important parameter for slip-line model because it determines the direction of the shear plane. According to Chandiramani et al. [29], the equivalent shear angle is affected by the instantaneous cutting direction and the waviness of the previous-cut surface. Zhu et al. [18] further validates that the changed cutting velocity also influence the shear angle. With the full consideration

the static and dynamic factors, the equivalent shear angle of UPDS can be expressed by:

$$\phi_{i,j} = \phi_d^{i,j} + \phi_p - arctan\left(\frac{dF(y_i)}{dy}\right) \tag{9}$$

where ϕ_p is the effective shear angle induced by the waviness of the previous-cut surface, which equals to 0 due to the smoothness of the original surface. According to Refs [18, 30], $\phi_d^{i,j}$ is the effective shear angle representing the effects of changed cutting velocity and frictional states in the deformation zone, which can be expressed by:

$$\phi_d^{i,j} = arctan\left(\frac{\zeta_1 \cos\gamma_0}{1-\zeta_1 \cos\gamma_0}\right) + arctan\left(\frac{\zeta_2 \cos\gamma_{i,j}}{1-\zeta_2 \cos\gamma_{i,j}}\right) \tag{10}$$

where ζ_1 and ζ_2 represent the equivalent ratios of the DoC to chip thickness.

Based on the geometrical relations as shown in Fig. 2, the velocity along the shear plane can be expressed by:

$$v_s^{i,j} = \frac{\cos\gamma_{i,j}}{cos(\phi_{i,j}-\gamma_{i,j})} v_r \tag{11}$$

The strain rate can be acquired by the empirical expression proposed by Oxley et al. [17, 31], whose effectiveness has been validated in prediction of cutting force in transient cutting process and can be formulated by:

$$\dot{\gamma}_s^{i,j} = \frac{C_0 v_s^{i,j}}{l_{\mathrm{AB}}^{i,j}} = \frac{C_0 v_s^{i,j} \sin\phi_d^{i,j}}{d_{i,j}} \tag{12}$$

where C_0 is a constant value that reflects the cutting condition and material properties. With the assumption of uniform shear strain rate in the deformation zone, the shear strain can be obtained and expressed by:

$$\gamma_s^{i,j} = \frac{\cos\gamma_{i,j}}{2\sin\phi_{i,j}\cos(\phi_{i,j}-\gamma_{i,j})} \tag{13}$$

The equivalent shear stress, strain and strain rate in the deformation zone can be calculated according to the well-known Von Mises Criterion as:

$$\tau_s = \frac{\sigma_s}{\sqrt{3}}, \gamma_s = \sqrt{3}\varepsilon_s, \dot{\gamma}_s = \sqrt{3}\dot{\varepsilon}_s \tag{14}$$

The constitutive relationship between the shear stress and the strain, strain rate and temperature can be built according to the well-accepted Johnson-Cook model. By combining the Von Mises Criterion and the Johnson-Cook model [32], the shear stress can be expressed by the following equation:

$$\tau_s = \frac{1}{\sqrt{3}}\left[A + B\left(\frac{\gamma_s}{\sqrt{3}}\right)^n\right]\left[1 + C\,ln\left(\frac{\dot{\gamma}_s}{\sqrt{3}}\right)\right]\left[1 - \left(\frac{T-T_0}{T_m-T_0}\right)^m\right] \tag{15}$$

where A is a constant related to the yield strength, B and C are the coefficients related to strength and strain rate, m and n denotes the thermal softening coefficient and strain hardening exponent, respectively, T, T_0 and T_m represent the working temperature, room temperature and the melting temperature, respectively.

The rise of temperature in the shear plane needs to be assessed to calculate the shear stress using Eq. (15). Due to the difficulties in measuring the reliable data of temperature in the cutting zone, mathematical models are normally served as the alternative solution. The rise of temperature inside the deformation zone is majorly determined by three thermophysical activities including thermal dissipation, heat generated by plastic deformation, and thermal convection [33]. Even though detailed thermal models have been proposed to estimate the distribution of temperature in the shearing zone, these models can make the estimation of cutting force more complicated. To simplify the force model, a modified Boothroyd's temperature model [34] is adopted here to assess the working temperature T. Noteworthy, the Boothroyd's model the has been demonstrated to be acceptable in assessing the working temperature with high quality for orthogonal cutting, which can be expressed by:

$$\Delta T = T - T_0 = \frac{(1-\beta)\cos\gamma_{i,j}}{\rho S \sin\phi_{i,j}\cos(\phi_{i,j}-\gamma_{i,j})}\tau_s \tag{16}$$

where β relates to the heat diffusion, ρ is the density and S is the specific heat of the workpiece material. Through incorporating Eq. (16) into Eq. (15), the shear stress in the shear band can be acquired.

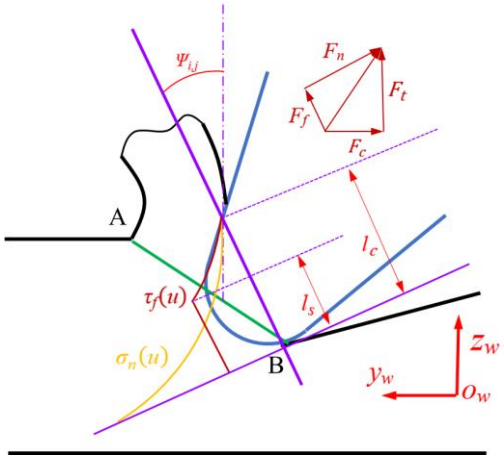

Fig. 3. Stress distribution on tool rake face in the slip-line model.

3.1.2 Calculation of shearing force

To calculate the shearing forces, the distribution of nominal stress and frictional stress along the

tool-chip interface should be determined in advance. According to Refs [35], the famous equilibrium equation of stress for the straight slip-line model is expressed as:

$$\frac{\partial \sigma}{\partial s_1} = \frac{\partial \tau}{\partial s_2} = \frac{\partial \tau}{\partial \gamma}\frac{\partial \gamma}{\partial t}\frac{\partial t}{\partial s_2} \tag{17}$$

where s_1 and s_2 are the distance along the shear band and vertical to shear band, respectively. As the shape of the shear band is assumed to be straight in the model, Eq. (17) can also be written as:

$$\frac{\sigma_{\mathrm{A}} - \sigma_{\mathrm{B}}}{l_{\mathrm{AB}}^{i,j}} = \frac{\partial \tau_s}{\partial \gamma_s}\frac{\partial t}{\partial s_2}\dot{\gamma}_s \tag{18}$$

where σ_{A} and σ_{B} are the hydrostatic stress on the two ends of the shear band, $l_{\mathrm{AB}}^{i,j}$ is the length of the shear band. As learned from Johnson-Cook model, the shear stress is the function of strain as shown in Eq. 15. Through differential method, it is can be obtained that:

$$\frac{\partial \tau_s}{\partial \gamma_s} = \frac{nB{\gamma_s}^{n-1}}{A\left(\sqrt{3}\right)^n + B{\gamma_s}^n}\tau_s \tag{19}$$

According to the geometrical relation of the slip-line model as shown in Fig. 3, following expressions can be acquired as:

$$l_{\mathrm{AB}}^{i,j} = \frac{d_{i,j}}{sin\,\phi_d^{i,j}}\ and\ \frac{\partial t}{\partial s_2} = \frac{1}{v_r\,sin\,\phi_{i,j}} \tag{20}$$

The boundary condition is derived based on the work by Oxley et al. [31], who suggests that the non-parallel relationship between the original surface and the cutting direction has a minimum impact on the boundary conditions. The shear stress at the end of the original surface can be expressed by:

$$\sigma_{\mathrm{A}} = \tau_s\left[1 + 2\left(\frac{\pi}{4} - \phi_{i,j}\right)\right] \tag{21}$$

Through combing the Eqs. (12), (13) and (18)-(21), the stress at point B can be derived as:

$$\sigma_{\mathrm{B}} = \sigma_{\mathrm{A}} - \frac{2\tau_s nC_0 B{\gamma_s}^n}{A\left(\sqrt{3}\right)^n + B{\gamma_s}^n} \tag{22}$$

Along the tool-chip interface, the highest nominal stress generates at the tool tip and gradually decreases to zero at separation point. The hydrostatic stress at point B should be equal to the highest nominal stress at tool tip, which can be served as the boundary condition, as shown in Fig. 3. Therefore, according to [30], the nominal stress distribution along the equivalent rake face from the lowest point of cutting edge can be expressed by:

$$\sigma_n(u) = \sigma_B\left[1 - \left(\frac{u}{l_c}\right)^a\right] \tag{23}$$

where u is the distance to the lowest point of the tool edge, a is the parameter that determine the stress distribution, l_c is the contact length between the generated chip and the equivalent tool rake face,

which can be expressed by [36]:

$$l_c = \frac{2d_{i,j}\cos\left(\phi_d^{i,j} - \gamma_e^{i,j}\right)}{\sin\phi_d^{i,j}} \tag{24}$$

Through integration method, the normal shearing force at the *i*-th CLP and the *j*-th discretized element can be calculated by the following expression as:

$$F_n^{i,j} = \int_0^{l_c} w_{i,j}\sigma_n(u)du = \frac{2a\cos\left(\phi_d^{i,j} - \gamma_e^{i,j}\right)}{(a+1)\sin\phi_d^{i,j}}\sigma_B w_{i,j}d_{i,j} \tag{25}$$

where $w_{i,j}$ denotes the width of the *j*-th discretized element.

As shown in Fig. 3, the frictional state between the tool rake face and the generated chip includes two types, namely the sticking and sliding state [12]. A two-state model is used to determine the distribution of frictional stress along tool-chip interface. The sticking friction generates at the region near the lowest point of the tool edge, and the frictional stress induced by the sticking effect remains constant. At the reminder of the tool-chip interface, the sliding friction occurs, and the frictional stress in this region is proportional to the normal shear stress [37]. Accordingly, based on Eq. (23), the frictional stress distribution over the tool-chip interface is mathematically expressed by:

$$\tau_f(u) = \begin{cases} \mu_e\sigma_B\left(1 - \left(\frac{l_s}{l_c}\right)^a\right) & 0 \le u \le l_s \\ \mu_e\sigma_n(u) & l_s < u \le l_c \end{cases} \tag{26}$$

where l_s denotes the sticking length and μ_e is the friction coefficient on tool rake face. To simplify the model, it is assumed that the sticking length is half of the tool-chip contact length. In the same way, the frictional shearing force at the *i*-th CLP and the *j*-th discretized element can be obtained by solving the following expression as:

$$F_f^{i,j} = \int_0^{l_s} w_{i,j}\mu_e\sigma_B(1 - 2^{-a})du + \int_{l_s}^{l_c} w_{i,j}\mu_e\sigma_n(u)du \tag{27}$$

As shown in Fig. 3, there is an inclination angle $\Psi_{i,j}$ between the equivalent rake face and the DoC direction, which can be obtained based on the geometrical relation as:

$$\Psi_{i,j} = \begin{cases} \arccos\left(\frac{l_c}{2r_e}\right) - \arctan\left(\frac{dF(y_i)}{dy}\right) & l_c \le l_e \\ \arcsin\left(\frac{r_e + r_e\sin\gamma_0}{l_c}\right) - \gamma_0 - \arctan\left(\frac{dF(y_i)}{dy}\right) & l_c > l_e \end{cases} \tag{28}$$

Accordingly, the cutting force and the thrust force at the *i*-th CLP and the *j*-th discretized element can be expressed as:

$$\begin{cases} F_{c,s}^{i,j} = F_n^{i,j} \cos \Psi_{i,j} + F_f^{i,j} \sin \Psi_{i,j} \\ F_{t,s}^{i,j} = F_n^{i,j} \cos \Psi_{i,j} - F_f^{i,j} \sin \Psi_{i,j} \end{cases} \tag{29}$$

3.2 Ploughing force model

When the DoC is lower than a critical threshold value, the ploughing mechanism becomes dominant in the material removal process of machining [38, 39]. In this case, the workpiece material experiences elastic deformation and flows beneath the tool edge. According to the indentation theory, the ploughing forces are calculated to be proportional to the instantaneous tool-workpiece interference volume. Due to the dynamic cutting process of UPDS, the tool-workpiece interference volume is not only determined by the instantaneous DoC, but also influenced by the dynamic clearance angle generated by the time varying cutting direction. Based on the geometrical relation, the equivalent clearance angle $\kappa_{i,j}$ at the *i*-th CLP and the *j*-th discretized element can be expressed by:

$$\kappa_{i,j} = \kappa_0 + arctan\left(\frac{dF(y_i)}{dy}\right) \tag{30}$$

where κ_0 is the tool clearance angle. With consideration of the width of the discretized orthogonal cutting element, the tool-workpiece interference volume is expressed by [28]:

$$V_{i,j} = \begin{cases} w_{i,j} r_e \left(\varsigma_{i,j} - \dfrac{\sin 2\varsigma_{i,j}}{2}\right) & d_{i,j} \le r_e\left(1 - \cos \kappa_{i,j}\right) \\ \dfrac{w_{i,j}}{2}\left[\begin{array}{c} {r_e}^2\left(\varsigma_{i,j} + \kappa_{i,j}\right) - r_e(r_e - d_c)\left(\sin \varsigma_{i,j} + \sin \kappa_{i,j}\right) \\ + \dfrac{\left(d_c - r_e + r_e \cos \kappa_{i,j}\right)^2}{\tan \kappa_{i,j}} \end{array}\right] & r_e\left(1 - \cos \kappa_{i,j}\right) < d_{i,j} \le d_c \end{cases} \tag{31}$$

with

$$\varsigma_{i,j} = arccos\left(1 - \frac{d_{i,j}}{r_e}\right) \tag{32}$$

where d_c is the critical chip thickness that separate the shearing and ploughing material removal mechanism. According to Lai et al. [40], the critical chip thickness is proportional to the tool edge radius, so d_c is approximate to be a constant value of $0.3r_e$ in this study.

Similar to the calculation of shearing force, the ploughing forces are calculated considering the inclination angle $\vartheta_{i,j}$ between thrust direction and *z*-axis as:

$$\begin{cases} F_{c,p}^{i,j} = u_p k_{int} V_{i,j} \cos \vartheta_{i,j} - k_{int} V_{i,j} \cos \vartheta_{i,j} \\ F_{t,p}^{i,j} = k_{int} V_{i,j} \cos \vartheta_{i,j} + u_p k_{int} V_{i,j} \sin \vartheta_{i,j} \end{cases} \tag{33}$$

with

$$\vartheta_{i,j} = -\arctan\left(\frac{dF(y_i)}{dy}\right) \tag{34}$$

where u_p denotes ploughing friction coefficient and k_{int} is the proportion ratio of the ploughing force. k_{int} can be determined through the assumption that the shearing force and the ploughing force at the critical chip thickness is continuous [18].

3.3 Calculation of the cutting force

The schematic illustration of the engagement area of the tool edge on the workpiece for the *i*-th CLP is shown in Fig. 4. A coordinate system o_t-$x_t y_t z_t$ is fixed on the tool rake face with $o_t z_t$ axis vertical to the original surface and passing through the CLP. As learned from the general surface formula of UPDS expressed in Eq. (1), the engaged region of the tool rake face is axisymmetric with respect to the $o_t z_t$ axis, so the angles of $\overline{o_i A}$ and $\overline{o_i B}$ with respect to $o_t z_t$ axis are expressed by:

$$\theta_a = -\theta_b = -\arctan\left(1 - \frac{F(y_i)}{R_t \cos\gamma_0}\right) \tag{35}$$

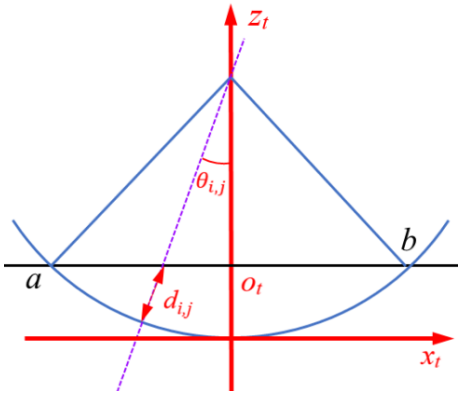

Fig. 4. Engagement area of the tool edge on the workpiece.

Through the discretization method, the engaged region is evenly divided into *N* orthogonal cutting elements. The practical DoC of the *j*-th discretized element is expressed by:

$$d_{i,j} = R_t \cos\gamma_0 - \frac{R_t \cos\gamma_0 - F(y_i)}{\cos\theta_{i,j}} \tag{36}$$

where $\theta_{i,j}$ is the relative angle of the *j*-th element to the $o_t z_t$ axis, which can be calculated by:

$$\theta_{i,j} = \theta_a - j\frac{2\theta_b}{N} \tag{37}$$

The corresponding width of the *j*-th element is expressed by:

$$w_{i,j} = R_t \frac{2\theta_b}{N} \tag{38}$$

In total, through summering the shearing and ploughing forces of all the discretized elements, the

overall cutting force and thrust force at the i-th CLP are expressed as:

$$\begin{cases} F_c^i = \sum \{F_{c,p}^{i,j} | \forall d_{i,j} < d_c\} + \sum \{F_{c,s}^{i,j} | \forall d_{i,j} \geq d_c\} \\ F_t^i = \sum \{F_{t,p}^{i,j} | \forall d_{i,j} < d_c\} + \sum \{F_{t,s}^{i,j} | \forall d_{i,j} \geq d_c\} \end{cases} \tag{39}$$

4. Experimental setup

Diamond sculpturing experiments for textured micro-grooves were conducted on a multi-axis ultra-precision machine (Moore 350FG, USA), as shown in Fig. 5. A single point diamond tool with the tool nose radius of 1.2 mm is used in the experiments. The rake and clearance angle of the tool is 0° and 7°, respectively. The tool edge radius is set at 40 nm that is the standard value of diamond tools. The workpiece material is brass. The content of Cu for the brass is nearly 68%, while the content of Zn ranges from 20% to 30%. In the sculpturing process, the workpiece is fixed on the locked spindle, while the diamond tool is mounted on the y slide. The kinematics of sculpturing and the textured surface generation mechanism are detailed in the section 2.

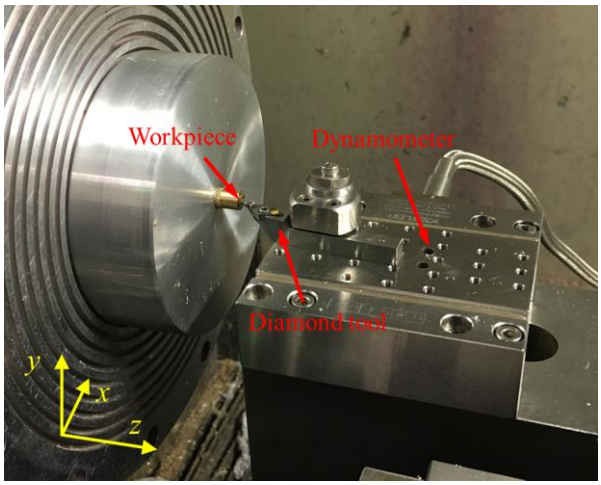

Fig. 5. Experiment setup for UPDS.

In UPDS of textured surfaces, the two important kinematic features of the cutting process are the position dependent depth of cut and time varying cutting directions, respectively. Harmonic micro-structures are the typical structure that is characterized as position dependent curvatures and varying DoCs. To validate the proposed model, two micro-textured harmonic grooves with different amplitudes and wave lengths were fabricated and the generated cutting force signals were collected. The general formula of the toolpath of the harmonic micro-grooves is expressed as:

$$z(y) = A_h \sin\left(\frac{2\pi}{l_h} y + \frac{\pi}{2}\right) - A_h - d_n \quad (40)$$

where A_h and l_h denotes the amplitude and the wavelength, and d_n is the nominal DoC. The coefficients and the machining parameters of the two micro-textured harmonic grooves are shown in Table 1. The generated surface topographies of the textured grooves and the corresponding micro-topographies were captured by an optical measurement system Zygo Nexviw with proper magnifications. The 3D geometric characteristics of the generated textured grooves and the corresponding micro-topographies of the bottom surfaces are shown in Fig. 6.

To capture the cutting force during cutting, the diamond tool is fixed on a three-channel dynamometer sensor (Kistler 9256C1), as shown in Fig. 5. A high sample frequency of 30 kHz was adopted to ensure the measurement accuracy of the cutting force signals. To remove the high-frequency noise coupled in the signals, a low frequency passing filter with a cut-off frequency of 1000 Hz is adopted after collecting the singles.

Table 1. Coeffecients and machining paramters for textured grooves.

Cutting parameters	Groove 1	Groove 2
Amplitude (μm)	4	2
Wave length (μm)	400	200
Nominal DoC (μm)	1	1
Cutting speed (mm/min)	20	20

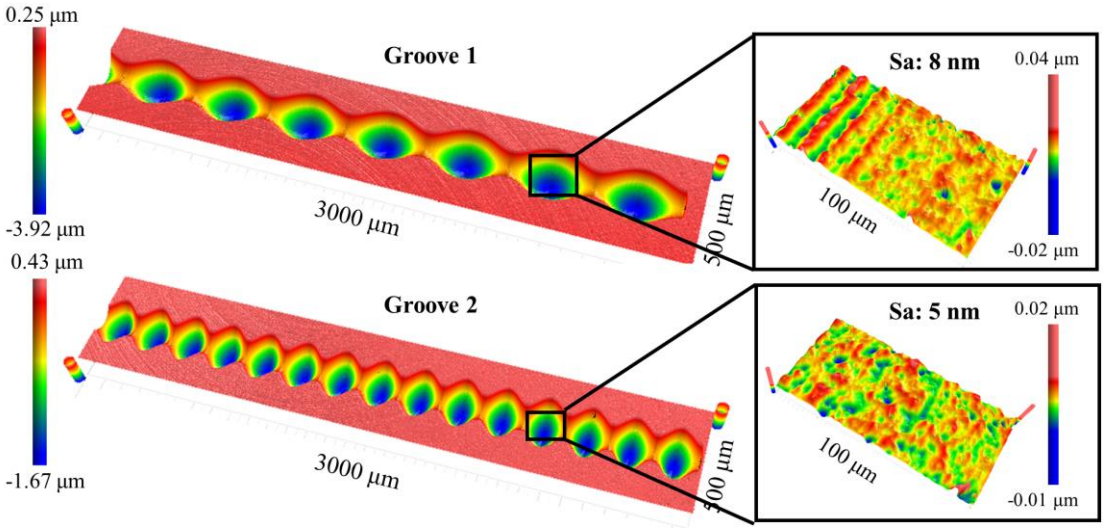

Fig. 6. 3D surface topographies of the generated micro-grooves and the corresponding micro-topographies.

5. Results and discussion

In this section, the oscillations induced dynamic material removal mechanism for UPDS is analyzed based on the simulation results of the proposed model, which is helpful to understand the cutting mechanisms for UPDS of textured surfaces. Besides, the effectiveness of the proposed model is demonstrated through comparing the estimated forces and the original forces measured in UPDS of two harmonic grooves with different dimension features.

5.1 Dynamic cutting mechanism

In UPDS of textured grooves, the *z*-axis experiences high-frequency front and back movements to generate the desired surfaces, which inevitably leads to the time varying DoC and cutting conditions. To clearly explain the dynamic cutting mechanism of UPDS, the sculpturing process for textured groove 1 is simulated based on the proposed model, and the relating coefficients and parameters are shown in Table 1.

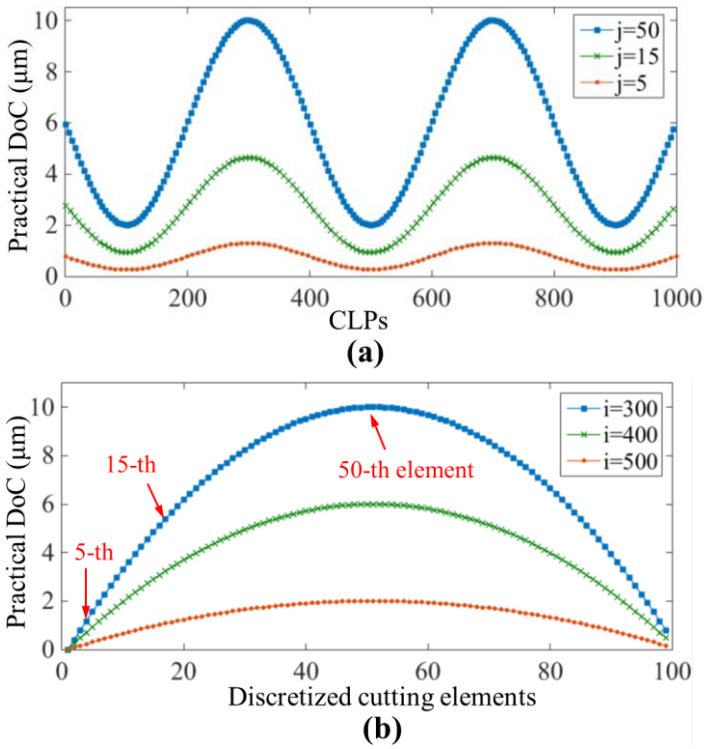

Fig. 7. The change of the practical DoC (a) for the 5-th, 15-th and 50-th discretized cutting elements with respect to the CLPs and (b) along tool edge at three different CLPs.

According to the proposed model, discretization method is applied on the tool edge, and each discretized element is treated as an independent orthogonal cutting process. The change of the practical

DoCs for the 5-th, 15-th and 50-th discretized cutting elements of tool edge is shown in Fig. 7 (a) with respect to the CLPs. It is observed that the practical DoC at the three discretized cutting elements changes at different CLPs along feed direction, which induces the time varying cutting directions. The variation of the angle between the time varying cutting direction and feed direction is shown in Fig. 8 (a). It is also observed from Fig. 7 (a) that the amplitude variation of DoC at the 50-th element is much larger than that at 5-th element, which indicates that the practical DoC of each element not only changes with respect to CLPs, but also is determined by its position on the tool edge. Fig. 7 (b) shows the change of the practical DoCs along tool edge at three different CLPs. At a specific CLP, the practical DoCs decreases from the middle to the two sides of tool-workpiece engagement area, due to the round shape of the tool edge. When the DoC is lower than the critical chip thickness, the material removal is dominated by ploughing mechanism instead of shearing [38]. Overall, it is learned that the kinematics of UPDS is characterized as the oscillations induced time varying cutting directions as well as the round-edged tool induced position dependent practical DoC, both of which highly influences the material removal process of UPDS.

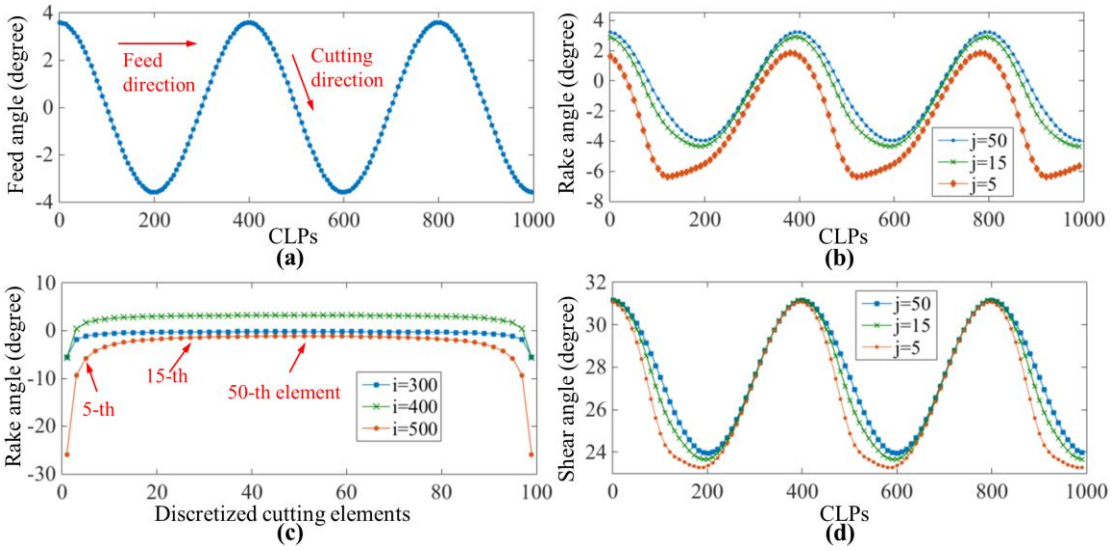

Fig. 8. The change of the (a) angle induced by time varying cutting direction, (b) equivalent rake angle for the 5-th, 15-th and 50-th discretized cutting elements with respect to the CLPs, (c) equivalent rake angle along tool edge and (d) shear angle with respect to the CLPs.

The variation of the equivalent rake angle defined by Eq. (6) is shown in Fig. 8 (b) with respect to CLPs. It is observed that the equivalent rake angle for the 50-th and 15-th element changes in a quasi-harmonic shape along feed direction. This is because the 50-th and 15-th orthogonal cutting

element is located near the middle of tool-workpiece engagement area, accordingly, having a relatively large practical DoC. In this case, the equivalent rake angle is majorly determined by the tool rake angle and the instantaneous cutting direction. In comparison, for the elements located near the sides (5-th element) whose practical DoCs are comparable to tool edge radius, the equivalent rake angle tends to be negative, as shown in Fig. 8 (c). Therefore, due to the dynamic cutting process of UPDS and the round-edged shape of the tool edge, the equivalent rake angle is dominated by three factors, namely cutting direction, tool rake angle and position on the tool edge. Similarly, the equivalent shear angle defined in Eq. (9) presents the similar variation trend with respect to CLPs, as shown in Fig. 8 (d). As the shear angle defines the plastic deformation direction in the cutting zone [12], it is learned that the dynamic cutting process of UPDS leads to the dynamic material removal mechanisms featuring time varying and position dependent plastic flow directions. As a result, the slip-line model with the consideration of these dynamic factors is required to accurately estimating the stress in the cutting zone.

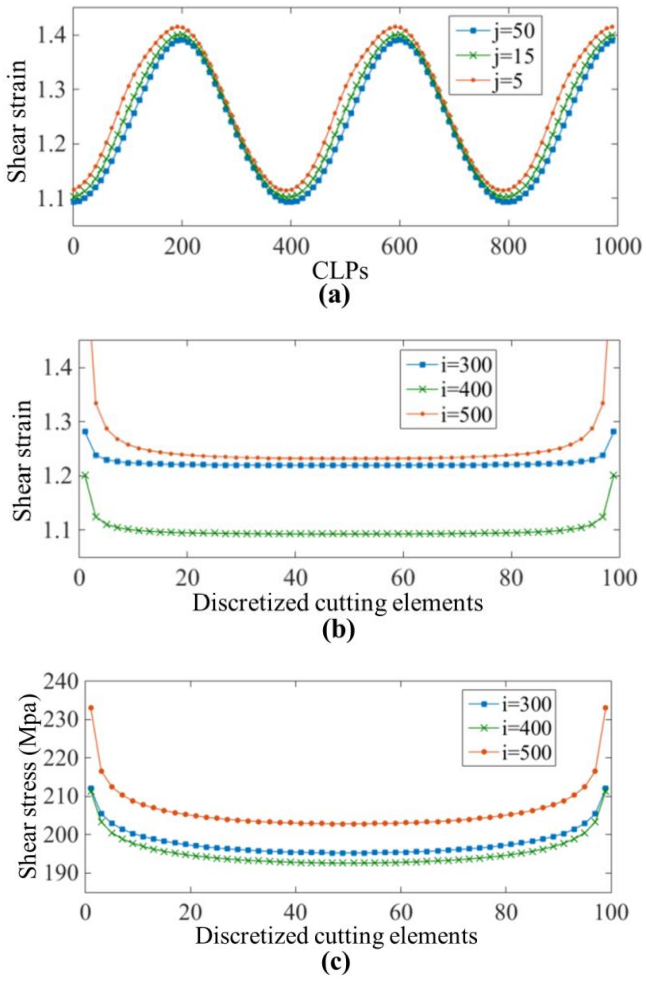

Fig. 9. The variation of the shear strain (a) with respect to the CLPs, (b) at different positions on the tool edge, and (c) the variation of shear stress at different positions on the tool edge.

Considering the dynamic equivalent rake angle and the equivalent shear angle, the variation of the shear strain defined by Eq. (13) and the positions on the tool edge are shown in Fig. 9 (a) with respect to CLPs. The distribution of the shear strain at different positions on the tool edge is shown in Fig. 9 (b) for the 300-th, 400-th and 500-th CLP. The change of the shear strain at different CLPs is attributed to the time varying cutting directions, while the change of the shear strain along tool edge is caused by the round-edged effect of the tool. As known from the Johnson-Cook model expressed by Eq. (15), the shear stress in the shear band is the function of the shear strain. As a result, the dynamic shear strain inevitably leads to the position dependent shear stress along tool edge as shown in Fig. 9 (c). Based on the proposed analytical model, the cutting force of each discretized elements are derived by the slip-line model considering the dynamic constitutive relations, as expressed in Eqs. (25) and (27). The simulation results well demonstrate that the proposed cutting force model can capture the dynamic material removal process of UPDS induced by the time varying cutting directions, position dependent DoCs and round-edged effect.

Table 2. Parameters relating to workpiece material properties and Johnson-Cook model.

A	9×10^7	T_m	1083 °C
B	2.92×10^8	T_0	25 °C
C	0.025	ρ	8.5 g/cm^3
m	1.09	S	445 J/kg·°C
n	0.31	β	0.4

Table 3. Parameters relating to analytical model.

γ_0	0	ζ_1	0.1
κ_0	7°	ζ_2	0.28
R_t	1.2 mm	μ_e	0.092
r_e	50 nm	μ_p	0.2
ξ	1.5	a	0.7
N	100	Δy	1 μm

5.2 Validation of the cutting force model

Referring to Refs [32, 41], the parameters relating to the workpiece material properties of brass and the Johnson-Cook model are presented in Table 2, the availability of which has been demonstrated

by researchers. The remaining parameters of the analytical model are shown in Table 3, some of which are identified by the training method. To be more specific, these parameters are reasonably preset in advance, then a period of original cutting force (about 0.3s) are selected to optimize these parameters through fine-tuning operation. Then, the proposed force model is experimentally validated through sculpturing two types of harmonic grooves whose coefficients are shown in Table 1.

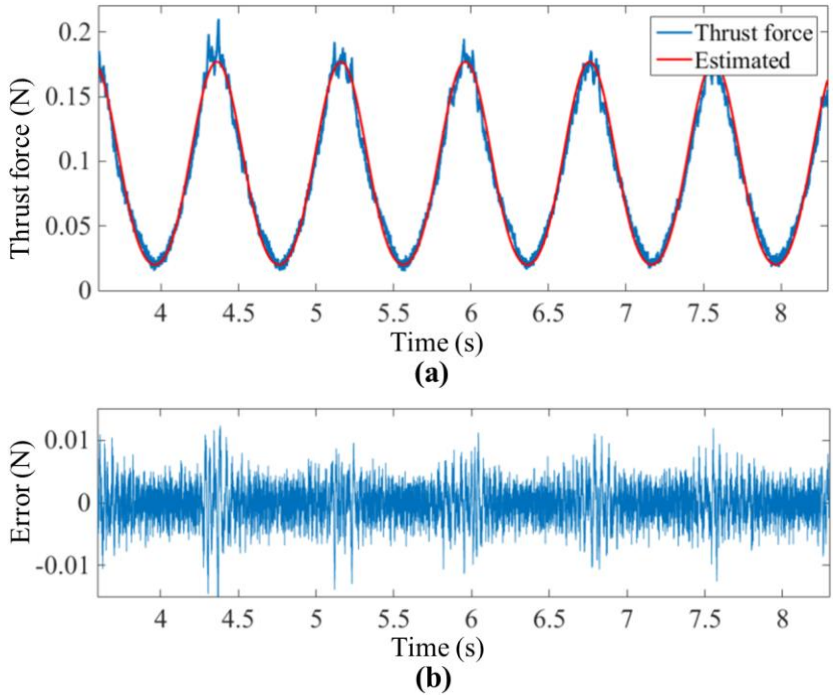

Fig. 10. (a) The estimated and measured thrust force for groove 1 and (b) predation error.

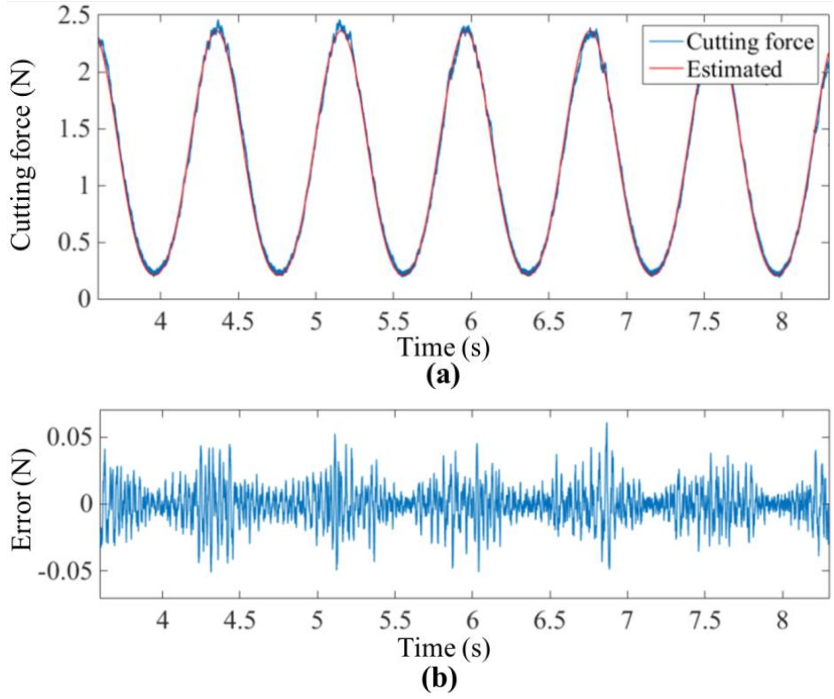

Fig. 11. (a) The estimated and measured cutting force for groove 1 and (b) predation error.

The estimated thrust force and cutting force for groove 1 are shown in Fig. 10 (a) and Fig. 11 (a), respectively, and the estimated forces are compared with the original forces collected in UPDS of groove 1. To eliminate the distraction of the high-frequency noise, the measured original forces are filtered by a low-pass filter with a cut-off frequency of 1000 Hz. As shown in Fig. 10 (a) and Fig. 11 (a), a good accordance of the experimental and estimated results is obtained for both thrust and cutting forces, which validates the effectiveness of the proposed analytical model. To quantitatively evaluate the estimation accuracy, the modelling errors of the thrust and cutting force are further shown in Fig. 10 (b) and Fig. 11 (b), respectively. The modelling errors of thrust force and cutting force are less than 0.01 N and 0.05 N, respectively, indicating a good estimation accuracy. The close agreement between the simulated and experimental results is mainly attributed to the comprehensiveness of the force model that not only considers the shearing and ploughing material removal mechanisms but also integrating the oscillated servo motions induced dynamic material removal mechanism into the force model. Apart from the forces generated from the material deformation, the sticking and sliding states of the chip on the tool rake face are also considered in the calculation of frictional forces.

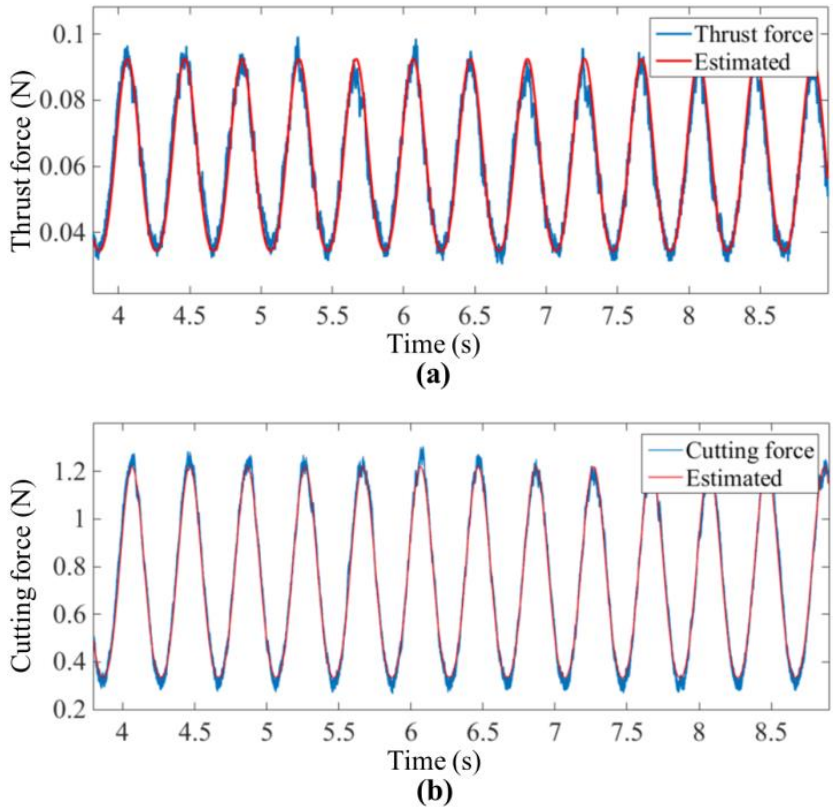

Fig. 12. The estimated and measured (a) thrust force and (b) cutting force for groove 2.

The model is further validated through modelling the thrust force and cutting force for groove 2 with lower wave length, as shown in Fig. 12 (a) and (b). Noteworthy, the lower harmonic wave length of groove 2 indicates the faster oscillated speed and more significant dynamic characteristics. As shown in Fig. 12 (a) and (b), both the amplitudes and the variation tendency of the estimated forces are well consistent with that of original ones, demonstrating that the proposed analytical model is effective to estimate the time varying cutting forces generated in UPDS of textured micro-grooves. As shown in Fig. 6, obvious tool oscillation marks can be observed on the micro-topography of groove 1, and leads to a larger surface roughness of 8 nm compared with that of groove 2. As learned from the simulation results, the easy tool vibrations in the UPDS of groove 1 are majorly attributed to the larger variation amplitudes of the cutting forces for groove 1. Especially, the tool oscillations marks are majorly distributed at the points where the cutting forces are discontinuous. Therefore, the investigation on the cutting force model is important and meaningful to improve the machined surface quality and optimizing the machining parameters.

The main advantage of the proposed model is that this model can accurately predict the dynamic cutting forces generated in cutting of textured surfaces, due to the consideration of the dynamic material removal mechanisms. The generation of the cutting force majorly results from the coupling effect between the material plastic deformation process and tool-workpiece interaction behaviors. More importantly, the proposed model is developed on the basis of the in-depth investigation on the dynamic material removal mechanism and tool-workpiece interaction behaviors, so the proposed model is universally applicable in other cases. As the grooves 1 and 2 belong to the typical harmonic structure featuring time varying DoCs and cutting direction, the good agreement of the estimated and experimental results also validates that the proposed model is applicable to the estimation of the time varying cutting forces in UPDS of various micro-structures. One important caveat of the proposed model is that some important should be identified by the training method.

6. Conclusions

In this study, a comprehensive analytical cutting force model was developed for ultra-precision diamond sculpturing (UPDS) of micro-grooves with textured surfaces. The dynamic material removal process induced by the oscillated servo motions is fully considered in the model through incorporating

the time varying equivalent rake angle, shear angle, clearance angle, strain and stress in the determination of shearing and ploughing forces. The interface between the chip and the tool rake face is divided into sticking and sliding sub-regions to calculate the frictional force. Moreover, discretization method is employed to determine the tool edge shape induced non-uniform distribution of cutting force along tool edge. To validate the proposed model, the predicted cutting forces are compared with that of measured ones for two types of harmonic micro-grooves with different amplitudes and wave lengths. The main conclusions of this work can be summarized as follows:

(1) The oscillated servo motions in UPDS lead to the time varying rake angle, which accordingly results in the variable strain and stress at each cutter location point (CLP). Attributing to these dynamic factors, the shearing force derived by slip-line theory is not only determined by the cutting speed and depth of cut (DoC) as conventional orthogonal cutting, but also influenced by the transient cutting direction in UPDS.

(2) According to the indentation theory, the ploughing force is calculated to be in direct proportion to the tool-workpiece interference volume. Similar to shearing force, the oscillated servo motion induced dynamic clearance angle also leads to the time varying ploughing forces in UPDS.

(3) Due to the round edge shape, the practical DoCs of each discretized segments are various along the tool edge, which results in a position-dependent shear stress and shear strain.

(4) The good agreement between the estimated and experimental results validates the effectiveness of the proposed model for estimating the cutting forces in UPDS of textured micro-grooves. Owing to the discretization method, the model also can be used to simulate the stress and force distribution on the tool edge.

Acknowledgement

This work was supported partially by the Research Committee of The Hong Kong Polytechnic University (Project Code: RUNS), Research Grant Council of the Hong Kong Special Administrative Region, China (Project No.PolyU152021/17E), and the National Science Foundation of China (NSFC) (Project No. 51675455).

References

[1] M. Wang, C. Zhao, X. Miao, Y. Zhao, J. Rufo, Y.J. Liu, T.J. Huang, Y. Zheng, Plasmofluidics: Merging Light and Fluids at the Micro-/Nanoscale, Small, 11 (2015) 4423-4444.

[2] Y. Xu, M. Shinomiya, A. Harada, Soft Matter-Regulated Active Nanovalves Locally Self-

Assembled in Femtoliter Nanofluidic Channels, Advanced Materials, 28 (2016) 2209-2216.
[3] J. Zhang, N. Suzuki, Y. Wang, E. Shamoto, Ultra-precision nano-structure fabrication by amplitude control sculpturing method in elliptical vibration cutting, Precision Engineering, 39 (2015) 86-99.
[4] Y.-L. Chen, Y. Cai, Y. Shimizu, S. Ito, W. Gao, B.-F. Ju, Ductile cutting of silicon microstructures with surface inclination measurement and compensation by using a force sensor integrated single point diamond tool, Journal of Micromechanics and Microengineering, 26 (2015) 025002.
[5] Z. Sun, S. To, S. Zhang, A novel ductile machining model of single-crystal silicon for freeform surfaces with large azimuthal height variation by ultra-precision fly cutting, International Journal of Machine Tools and Manufacture, (2018).
[6] Y.-L. Chen, Y. Cai, K. Tohyama, Y. Shimizu, S. Ito, W. Gao, Auto-tracking single point diamond cutting on non-planar brittle material substrates by a high-rigidity force controlled fast tool servo, Precision Engineering, 49 (2017) 253-261.
[7] G. Herrera-Granados, N. Morita, H. Hidai, S. Matsusaka, A. Chiba, K. Ashida, I. Ogura, Y. Okazaki, Development of a non-rigid micro-scale cutting mechanism applying a normal cutting force control system, Precision Engineering, 43 (2016) 544-553.
[8] X. Zhou, R. Wang, Q. Liu, Study on suppressing cutting force fluctuations based on chip loads for turning optical freeform surfaces, The International Journal of Advanced Manufacturing Technology, 90 (2017) 2037-2046.
[9] J. Weng, K. Zhuang, D. Chen, S. Guo, H. Ding, An analytical force prediction model for turning operation by round insert considering edge effect, International Journal of Mechanical Sciences, 128 (2017) 168-180.
[10] M. Kaymakci, Z. Kilic, Y. Altintas, Unified cutting force model for turning, boring, drilling and milling operations, International Journal of Machine Tools and Manufacture, 54 (2012) 34-45.
[11] G.C. Verma, P.M. Pandey, U.S. Dixit, Modeling of static machining force in axial ultrasonic-vibration assisted milling considering acoustic softening, International Journal of Mechanical Sciences, 136 (2018) 1-16.
[12] D. Germain, G. Fromentin, G. Poulachon, S. Bissey-Breton, From large-scale to micromachining: A review of force prediction models, Journal of Manufacturing Processes, 15 (2013) 389-401.
[13] N. Grossi, L. Sallese, A. Scippa, G. Campatelli, Speed-varying cutting force coefficient identification in milling, Precision Engineering, 42 (2015) 321-334.
[14] Y. Yan, J. Xu, M. Wiercigroch, Modelling of regenerative and frictional cutting dynamics, International Journal of Mechanical Sciences, (2019).
[15] H. Wang, Y. Hu, W. Cong, Z. Hu, A Mechanistic Model on Feeding-Directional Cutting Force in Surface Grinding of CFRP Composites using Rotary Ultrasonic Machining with Horizontal Ultrasonic Vibration, International Journal of Mechanical Sciences, (2019).
[16] M.E. Merchant, Mechanics of the metal cutting process. I. Orthogonal cutting and a type 2 chip, Journal of applied physics, 16 (1945) 267-275.
[17] P. Oxley, Development and application of a predictive machining theory, Machining Science and Technology, 2 (1998) 165-189.
[18] Z. Zhu, S. To, W.-L. Zhu, P. Huang, X. Zhou, Cutting forces in fast-/slow tool servo diamond turning of micro-structured surfaces, International Journal of Machine Tools and Manufacture, 136 (2019) 62-75.
[19] B. Li, Y. Hu, X. Wang, C. Li, X. Li, An analytical model of oblique cutting with application to end milling, Machining Science and Technology, 15 (2011) 453-484.

[20] J. Weng, K. Zhuang, D. Zhu, S. Guo, H. Ding, An analytical model for the prediction of force distribution of round insert considering edge effect and size effect, International Journal of Mechanical Sciences, 138 (2018) 86-98.
[21] Z. Fu, X. Chen, J. Mao, T. Xiong, An analytical force mode applied to three-dimensional turning based on a predictive machining theory, International Journal of Mechanical Sciences, 136 (2018) 94-105.
[22] L. Jieqiong, H. Jinguo, Z. Xiaoqin, H. Zhaopeng, L. Mingming, Study on predictive model of cutting force and geometry parameters for oblique elliptical vibration cutting, International Journal of Mechanical Sciences, 117 (2016) 43-52.
[23] N. Fang, I. Jawahir, P. Oxley, A universal slip-line model with non-unique solutions for machining with curled chip formation and a restricted contact tool, International Journal of Mechanical Sciences, 43 (2001) 557-580.
[24] D.J. Waldorf, R.E. DeVor, S.G. Kapoor, A slip-line field for ploughing during orthogonal cutting, Journal of Manufacturing Science and Engineering, 120 (1998) 693-699.
[25] H.-T. Young, P. Mathew, P. Oxley, Predicting cutting forces in face milling, International Journal of Machine Tools and Manufacture, 34 (1994) 771-783.
[26] L. Pang, A. Hosseini, H. Hussein, I. Deiab, H. Kishawy, Application of a new thick zone model to the cutting mechanics during end-milling, International Journal of Mechanical Sciences, 96 (2015) 91-100.
[27] J. Manjunathaiah, W. Endres, A study of apparent negative rake angle and its effect on shear angle during orthogonal cutting with edge-radiused tools, TRANSACTIONS-NORTH AMERICAN MANUFACTURING RESEARCH INSTITUTION OF SME, (2000) 197-202.
[28] M.P. Vogler, S.G. Kapoor, R.E. DeVor, On the modeling and analysis of machining performance in micro-endmilling, Part II: Cutting force prediction, Journal of manufacturing science and engineering, 126 (2004) 695-705.
[29] N.K. Chandiramani, T. Pothala, Dynamics of 2-dof regenerative chatter during turning, Journal of sound and vibration, 290 (2006) 448-464.
[30] T. Özel, E. Zeren, A methodology to determine work material flow stress and tool-chip interfacial friction properties by using analysis of machining, Journal of manufacturing science and Engineering, 128 (2006) 119-129.
[31] P. Oxley, W. Hastings, Predicting the strain rate in the zone of intense shear in which the chip is formed in machining from the dynamic flow stress properties of the work material and the cutting conditions, Proceedings of the Royal Society of London. A. Mathematical and Physical Sciences, 356 (1977) 395-410.
[32] G.R. Johnson, A constitutive model and data for materials subjected to large strains, high strain rates, and high temperatures, Proc. 7th Inf. Sympo. Ballistics, (1983) 541-547.
[33] T.J. Burns, M.A. Davies, Nonlinear dynamics model for chip segmentation in machining, Physical Review Letters, 79 (1997) 447.
[34] I. Administration, E.P.G.A.M. Group, G. Boothroyd, Temperatures in orthogonal metal cutting, Proceedings of the Institution of Mechanical Engineers, 177 (1963) 789-810.
[35] P.L.B. Oxley, H.-T. Young, The mechanics of machining: an analytical approach to assessing machinability, in, Chichester, England: Ellis Horwood Publisher, 1990.
[36] A. Toropov, S.-L. Ko, Prediction of tool-chip contact length using a new slip-line solution for orthogonal cutting, International Journal of Machine Tools and Manufacture, 43 (2003) 1209-1215.

[37] X. Jin, Y. Altintas, Prediction of micro-milling forces with finite element method, Journal of Materials Processing Technology, 212 (2012) 542-552.
[38] Z. Sun, S. To, S. Zhang, G. Zhang, Theoretical and experimental investigation into non-uniformity of surface generation in micro-milling, International Journal of Mechanical Sciences, 140 (2018) 313-324.
[39] N. Chen, L. Li, J. Wu, J. Qian, N. He, D. Reynaerts, Research on the ploughing force in micro milling of soft-brittle crystals, International Journal of Mechanical Sciences, (2019).
[40] X. Lai, H. Li, C. Li, Z. Lin, J. Ni, Modelling and analysis of micro scale milling considering size effect, micro cutter edge radius and minimum chip thickness, International Journal of Machine Tools and Manufacture, 48 (2008) 1-14.
[41] N. Fang, Sensitivity analysis of the material flow stress in machining, in: ASME 2003 International Mechanical Engineering Congress and Exposition, American Society of Mechanical Engineers, 2003, pp. 23-32.